Pan-cancer association of DNA repair deficiencies with whole-genome mutational patterns

Simon G. Sørensen[1,2], Amruta Shrikhande[3], Gustav A. Poulsgaard[1,2], Mikkel H. Christensen[1,2], Johanna Bertl[1,2], Eva R. Hoffmann[3]* and Jakob S. Pedersen[1,2,4]*

[1]Department of Molecular Medicine (MOMA), Aarhus University Hospital, Palle Juul-Jensens Boulevard 99, 8200, Aarhus N, Denmark.

[2]Department of Clinical Medicine, Aarhus University, Palle Juul-Jensens Boulevard 82, 8200, Aarhus N, Denmark.

[3]DNRF Center for Chromosome Stability, Department of Cellular and Molecular Medicine, Faculty of Health and Medical Sciences, University of Copenhagen, Denmark

[4]Bioinformatics Research Center (BiRC), Aarhus University, 8000, Aarhus C, Denmark.

*corresponding authors: jakob.skou@clin.au.dk, eva@sund.ku.dk

ABSTRACT

DNA repair deficiencies in cancers may result in characteristic mutational patterns, as exemplified by deficiency of *BRCA1/2* and efficacy prediction for PARP-inhibitors. We trained and evaluated predictive models for loss-of-function (LOF) of 145 individual DDR genes based on genome-wide mutational patterns, including structural variants, indels, and base-substitution signatures. We identified 24 genes whose deficiency could be predicted with good accuracy, including expected mutational patterns for *BRCA1/2*, *MSH3/6*, *TP53*, and *CDK12* LOF variants. *CDK12* is associated with tandem-duplications, and we here demonstrate that this association can accurately predict gene deficiency in prostate cancers (area under the ROC curve=0.97). Our novel associations include mono- or biallelic LOF variants of *ATRX, IDH1, HERC2, CDKN2A, PTEN,* and *SMARCA4,* and our systematic approach yielded a catalogue of predictive models, which may provide targets for further research and development of treatment, and potentially help guide therapy.

Keywords: DNA damage response, repair deficiency, predictive modelling, personalised medicine, mutational signatures.

LIST OF ABBREVIATIONS

AUROC | Area under the receiver operator characteristic

CNS | Central nervous system

DDR | DNA damage response

HMF | Hartwig medical foundation

HRD | Homologous recombination deficiency

Indel | Insertion or deletion

LASSO | least absolute shrinkage and selection operator

LASSO regression | Logistic regression with LASSO regularisation

LOF | Loss of function

LOH | Loss of heterozygosity

MMR | Mismatch repair

MSI | Microsatellite instability

PCAWG | Pan-cancer analysis of whole genomes

PR-AUC | Precision-recall area under the curve

PR-AUC-E | Precision-recall area under the curve enrichment from baseline

SBS | Single base substitution

SV | Structural variant

UV | Ultraviolet

VUS | Variants of unknown significance

WGS | Whole genome sequence

WT | Wild type

-d | Deficiency

INTRODUCTION

The DNA damage response (DDR) and repair pathways are central to the genetic integrity of cells, and deficiencies may cause mutational patterns genome-wide[1–3]. Some DNA repair deficiencies are known to modulate the response to therapies: *BRCA1/2* deficiency renders cancers susceptible to treatment with PARP inhibitors[4], mismatch repair-deficient cancers are sensitive to checkpoint inhibitors[5] but resistant to alkylating agents such as temozolamide[6], and *CDK12*-mutated cancers have a suggested sensitivity to CHK1 inhibitors[7]. Because of this, efforts have been made to annotate inactivating mutations in DDR genes[8]. However, the approach is limited by the lack of functional impact annotation of most variants, which are generally denoted as “variants of unknown significance” (VUS). Moreover, loss of gene activity could also occur by other means, such as transcriptional silencing.

A complementary approach is to investigate whether DNA repair deficiencies can be identified by DNA mutational patterns, also referred to as ‘mutational scars’. This approach has been pioneered for homologous recombination deficiency caused by *BRCA1/2* deficiencies (-d), which can be successfully predicted by measuring the accumulation of small deletions with neighbouring microhomologous sequences[2,9,10], such as done by the HRDetect algorithm by Davies *et al.*[9]. The association with microhomologous deletions is due to the use of microhomology-mediated endjoining (MMEJ) to repair double-strand breaks in homologous recombination (HR) deficient tumours[11,12]. Likewise, mismatch repair-deficiency causes an elevated rate of mono- and dinucleotide repeat indels genome-wide, a genetic phenotype denoted microsatellite instability[13,14]. Mutations in other DNA repair genes have also been associated with mutational patterns, including the tumour suppressor gene *TP53*, which is associated with increased structural rearrangements and whole genome duplications[15,16] *CDK12* which is associated with a genome-wide phenotype of large tandem duplications[17,18].

86 The scope of this approach can now be evaluated systematically across DDR genes by
87 exploiting available whole cancer genomes from thousands of patients[19,20].
88
89 To achieve this, mutations observed genome-wide may be condensed into mutational summary
90 statistics for predictive modelling, including statistics based on single-base substitutions (SBS),
91 indels, and different types of structural variants (SV). The SBSs are statistically assigned to so-
92 called SBS signatures that are catalogued and enumerated within the COSMIC database[21].
93 Some of these are associated with specific DNA repair deficiencies as well as genotoxic
94 exposures, such as ultraviolet (UV) light and smoking. Each SBS signature captures the relative
95 frequency of the different mutation types and their flanking nucleotides[22].
96
97 Here we performed a systematic screen for DDR gene deficiencies that can be predicted
98 through their association with genome-wide mutational patterns. We developed a generic
99 approach to train predictive statistical models that identify associations with individual mutational
100 summary statistics that capture the mutational patterns, including SBS signatures, indels, and
101 large SVs. We applied it to 736 DDR gene deficiencies, considering both monoallelic and
102 biallelic loss of function (LOF), identified across 32 cancer types, in a combined set of whole
103 cancer genomes from 6,065 patients[19,20]. The underlying aim was to identify novel associations
104 with potential biological relevance and to evaluate whether DDR deficiencies can be predicted
105 with sufficiently high certainty to have a potential for clinical application.
106
107 Our analysis revealed 24 DDR genes where deficiencies are associated with specific mutational
108 summary statistics in individual cancer types across 48 predictive models. These results
109 recapitulated the expected associations between mutational patterns and deficiencies of
110 *BRCA1/2, TP53, MSH3/6,* and *CDK12*. We supplemented this knowledge by providing a

111 predictive model of *CDK12* deficiency that achieved high accuracy (area under the receiver
112 operator characteristic (AUROC) = 0.97) in prostate cancer. Furthermore, we present
113 unexpected predictive models of several DDR deficiencies; *ATRX* and *IDH1* deficiency in
114 cancers of the central nervous systems, *HERC2* and *CDKN2A* deficiency in skin, *PTEN*
115 deficiency in cancers of the central nervous system and uterus, and *SMARCA4* deficiency in
116 cancers of unknown primary.
117
118 **RESULTS**
119 **DDR gene deficiencies across 6,065 whole cancer genomes**
120 We compiled and analysed 2,568 whole genome sequences (WGS) from The Pan-Cancer
121 Analysis of Whole Genomes (PCAWG)[19] and 3,497 WGS from the Hartwig Medical Foundation
122 (HMF)[20]. In total we investigated 6,065 whole cancer genomes of 32 cancer types (**Fig. 1a;**
123 **Additional file 1, Supplementary Table 1**).
124
125 For each genome, we evaluated 736 known DNA damage response (DDR) genes for both
126 germline and somatic loss of function (LOF) events[23–25]. We annotated both mono- and biallelic
127 loss-of-function (LOF) events, where each event could be either a single nucleotide variant, an
128 indel, or a loss-of-heterozygosity (LOH) (**Fig. 1b,c; Additional file 1, Supplementary Table 2**).
129 Pathogenicity of single base substitutions (SBSs) and indels was evaluated using a combination
130 of CADD scores (>25; 0.3% most pathogenic variants) [26] and ClinVar annotation, when
131 available (**Methods**).
132
133 We inferred a total of 8,408 biallelic DDR gene deficiencies, primarily through a combination of
134 somatic or germline variants (SBSs and indels) with pathogenic potential (n=1,702), or LOH
135 events combined with a single pathogenic germline (n=3,562) or somatic (n=3,078) variant

136 (SBS or indel; **Fig. 1b**). On average we observed a single, biallelic DDR gene loss per patient,
137 with some tumours showing extreme rates of somatic pathogenic mutations (**Fig. 1c**). As
138 expected, *TP53* deficiency (*TP53*-d) was the most frequent LOF event (81 biallelic and 1,746
139 monoallelic events; 29% of tumours affected; **Additional file 1, Supplementary Table 2; Fig.**
140 **1d**), while 70% of DDR genes had biallelic deficiency in less than ten tumours across all cancer
141 types (511/736; **Fig. 1d**). Among monoallelic events, we identified 15,063 pathogenic germline
142 (59%) and 10,336 somatic (41%) events.
143
144 **Whole genome mutational patterns**
145 We collected mutational summary statistics for each cancer genome, which were used as
146 features for the downstream predictive models (**Fig. 1e,f; Additional file 2, Supplementary**
147 **Table 3-4**). For SBSs, we evaluated exposure towards predefined sets of cohort-specific SBS
148 signatures[22,27]. Short indels and SVs were simply categorised and counted: Deletions were sub-
149 categorised based on surrounding sequence repetitiveness and presence of microhomology.
150 SVs were sub-categorised by type (tandem duplications, inversions, deletions, and
151 translocations), five size ranges (not relevant for translocations), and cluster presence
152 (**Methods**). Several SBS signatures as well as some types of indels have suggested etiologies
153 (collected in **Additional file 1, Supplementary Table 5)**.
154
155 **Statistical modelling of DDR gene deficiencies**
156 For the downstream statistical analysis, we restricted our focus to DDR genes in cancer types
157 with more than five biallelic LOF events in either PCAWG or HMF (n=194) or more than ten
158 monoallelic LOF events (n=341) (**Additional file 1, Supplementary Table 6**). Using *BRCA2*-d
159 in the set of HMF breast cancer tumours (n=645) as an example, we observed biallelic LOF
160 events in 17 (2.6%; 14 germline, 3 somatic) tumours and monoallelic LOF events in 7 (1.1%; 4

germline, 3 somatic) tumours (**Additional file 1, Supplementary Table 8**). We further observed variants of unknown significance (VUS) events in 53 tumours (8.2%; 42 germline, 11 somatic), which were excluded from the analysis. The remaining *BRCA2* wild-type (WT) tumours (n=568; 88.1%) were used as a background set for training the predictive models (**Fig. 2a)**. The high fraction of germline pathogenic variants diminishes the probability of a reverse-causal relationship between the loss of *BRCA2* and the associated mutation patterns.

For each of the 535 groups of tumours we trained a LASSO regression model and evaluated the ability to discriminate between deficient and WT tumours (**Methods**). For *BRCA2*-d we observed a strong association with the number of deletions at sites of microhomology (**Fig. 2b**), with a median of 608 deletions per patient in *BRCA2*-d breast cancers versus 81 in *BRCA2* WT breast cancers, in agreement with prior findings[2,9,10]. The LASSO regression also included non-clustered inversions 10-100Kb and clustered tandem duplications 1−10Kb, although both show high variance among tumours for both deficient and WT (**Fig. 2b**) and have considerably smaller coefficients, ultimately contributing little influence on overall predictive performance (**Fig. 2c**).

Notably, some models include features with negative coefficients. The biologically interpretation would be that tumours with a certain gene deficiency have fewer mutations attributed to a particular mutation pattern. Negative features were excluded in the development of the HRDetect algorithm[9], but we include them as we cannot rule out the possibility that a DDR deficiency protects from specific types of mutagenesis. Though not distinguishable in this study, we suggest that negative coefficient features may derive in three ways: First, they may stem from enhanced repair; second, they may stem from the decomposition of mutation counts into

signatures; and third, the mutated tumours may represent a subclass of patients in terms of age, gender, or tumour subtype with specific mutational patterns.

Evaluating model performance

For each model, we evaluated the predictive performance using the area-under-the-receiver-operating-curve (AUROC) score as well as the precision-recall area-under-the-curve (PR-AUC) score. The PR-AUC score is a more robust measure for unbalanced data sets [28]; however, the expected value for non-informative (unskilled) models equals the fraction of true positives and thus varies between models. Therefore, we used the PR-AUC enrichment over the true-positive rate (PR-AUC-E) as our selection criteria for predictive models. For the downstream analysis, we included (shortlisted) models with PR-AUC-E that was substantial (>0.2; more than two standard deviations above the mean across all 535 models) and significant (Benjamin-Hochberg false discovery rate, FDR<0.05; Monte Carlo simulations) (**Methods**; **Additional file 1, Supplementary Table 7**). In addition, we tested each model in the same cohort in the other data set whenever one or more tumours had mono- or biallelic loss of the gene. Due to the difference in biology between the two sets, we did not use this to explicitly evaluate the predictive performance of models but have included the PR-AUC-E values from the tests in **Supplementary Table 6 and 7**.

In the example of *BRCA2*-d in breast cancers of the HMF data set, our model achieved an AUROC of 0.93 and a PR-AUC-E of 0.29 (**Fig. 2d,e; Additional file 1, Supplementary Table 7**). Out of 30,000 permuted LOF-sets, none had a similar or higher PR-AUC score and we considered the model significant with a p-value < $3x10^{-5}$ (FDR adjusted q-value < $6x10^{-4}$) (**Fig. 2f,g**). The model achieved a PR-AUC-E of 0.37 when tested on the PCAWG data set, suggesting that the model may generalise across both metastatic and non-metastatic tumours.

210 This was further supported by the independent discovery of a similar model in the PCAWG data
211 set, which had an almost similar predictive power in the HMF data (PR-AUC-E = 0.19;
212 **Supplementary Table 7**). Notably, the *BRCA2*-d model did not include non-clustered deletions
213 <100Kb, SBS signature 3, and SBS signature 8, all features which have been associated with
214 BRCAness[9]. However, SBS signature 3 and non-clustered deletions 1-10Kb are included in the
215 model when the deletions at sites of microhomology are omitted from the input data set,
216 suggesting that they are excluded during feature selection due to high positive correlation with
217 the number of deletions at sites of microhomology among HMF breast cancers (Pearson corr. >
218 0.7; **Fig. 2h**; **Additional file 1, Supplementary Table 9**).
219
220 Our selection criteria resulted in 48 shortlisted predictive models across 24 DDR genes (**Fig. 3a;**
221 **Additional file 1, Supplementary Table 7)**. As exemplified for *BRCA2*, each model is specified
222 by a set of predictive features representing mutational patterns associated with DDR gene LOF**.**
223 We divided the models into four groups based on aetiology and origin: models of *BRCA1/2*-d
224 (eight models of *BRCA2*-d and a single model of *BRCA1*-d; **Fig. 3b**); models of monoallelic
225 *TP53*-d (11 models; **Fig. 3c**); models of various monoallelic gene deficiencies derived from
226 colorectal cancer patients (eight models; **Fig. 3d**); and models including other DDR genes and
227 cancer types, including previously undescribed associations (20 models; **Fig. 3e**).
228
229 **Recapitulation and predictive modelling of expected associations with *BRCA1/2***
230 **deficiency**
231 Five models predicted biallelic loss of *BRCA2* in cancers of the ovary, prostate, pancreas, and
232 breast. In addition, three models predicted *BRCA2* monoallelic loss in cancers of the pancreas,
233 breast, and prostate. Finally, we derived a single model of biallelic *BRCA1* loss in ovarian

234 cancer (**Fig. 3c; Fig. 4a**). All models significantly outperformed their Monte-Carlo simulations
235 (q<0.05; Benjamini Hochberg FDR control) and had PR-AUC-E above 0.2 (**Fig. 4b,c**).
236
237 All *BRCA2*-d models were predominantly predicted by deletions at sites of microhomology,
238 consistent with the role of *BRCA2* in homologous recombination and suppression of
239 microhomology-mediated end joining[29]. Both clustered and non-clustered tandem duplications in
240 the range of 1 to 100Kb were included as features for various models, though with much smaller
241 predictive power. This agrees with what was identified for *BRCA2* deficient tumours in prior
242 studies[9,10]. The biallelic breast cancer model based on PCAWG further included SBS signature
243 3 as a predictive feature (**Fig. 4d**). Contrasting to the models of *BRCA2*-d, *BRCA1*-d in ovarian
244 cancer was exclusively associated with clustered and non-clustered tandem duplications (1-
245 10Kb; **Fig. 4d**). This aligns with prior studies[9,10]**,** which also found *BRCA1*-d to be closely
246 associated with a tandem-duplicator phenotype. In general, *BRCA1* and *BRCA2* were subject to
247 predominantly germline pathogenic events, and not a single deletion at a site of
248 microhomology, suggesting the expected forward causality (**Supplementary Table 8**). As for
249 the loss of *BRCA2*, the model for loss of *BRCA1* loss in ovary had sufficient predictive power
250 (PR-AUC-E = 0.3) in the other data set, suggesting that the model works independently of the
251 metastatic capacity of the tumour (**Supplementary Table 7**).
252
253 ***TP53* deficiencies associate with increased numbers of structural variants**
254 We detected 11 predictive models (four based on PCAWG and seven on HMF) of monoallelic
255 *TP53*-d across cancers of the breast, skin, ovary, uterus, neuro-endocrine tissues (NET), biliary
256 gland, head and neck, pancreas, and the central nervous system (CNS) (**Fig. 4e**). These
257 predictive models performed with PR-AUC-E values ranging from 0.21 to 0.48 in breast and
258 biliary gland cancers, respectively. Similarly, AUROC values ranged from 0.48 to 0.88, again in

259 breast and biliary gland cancers (**Fig. 4f,g**). In line with existing literature[30], *TP53-d* is
260 associated with a significantly increased number of structural variants across the genome
261 (Wilcoxon rank-sum test; **Fig. 4h,i**), except in skin cancers. The models of *TP53* loss in head
262 and neck, skin, breast, and the biliary gland performed well (PR-AUC-E above 0.2) in the other
263 data set, suggesting that the predictive performance generalises independent of metastatic
264 tumour state (**Supplementary Table 7**).
265
266 **Colorectal cancer models derived from hypermutated mismatch repair deficient tumours**
267 In the HMF colorectal cancers, we discovered eight predictive gene deficiency models (*MSH3,*
268 *SMC2, SMC6, BMPR2, CLASP2, SRCAP*, *UBR5,* and *UVRAG)* of monoallelic LOF with PR-
269 AUC-E ranging from 0.21 (*CLASP2*) to 0.62 (*MSH3*) (AUROC ranging from 0.68 for *SRCAP*
270 deficiency to 0.94 for *MSH3* deficiency; **Fig. 4j,k,l**).
271
272 We suggest that the high number of models of monoallelic deficiencies may arise from spurious
273 LOF events in DDR genes in a subset of colorectal cancers that are hypermutated. Some
274 colorectal cancers are signified by mismatch repair deficiencies, such as LOF of *MSH3* or
275 *MSH6*, creating a high number of deletions in repetitive DNA[13,14]. Indeed, we found that this
276 pattern was most profound among the *MSH3* mutated cancers (**Fig. 4m,n**). Furthermore, we
277 found co-mutation with *MSH3* across the tumours underlying each model, ranging from 20%
278 (*SRCAP*) to 33% (*BMPR2*) of the mutated tumours (**Fig. 4p**). This suggests that the models
279 (except for the model of *MSH3*-d) might be the consequence of the hypermutator phenotype. In
280 other words, the causality may be reversed in these cases, and the mutational process driven
281 by *MSH3*-d may have caused the majority of their LOF events. This notion is supported by
282 investigating the features of the models. All eight models are characterised by a single, primary
283 predictive feature: Insertions (*SMC2, SMC6, BMPR2, UBR5, and UVRAG*), deletions in

284 repetitive DNA (*MSH3, SRCAP*), or deletions not flanked by repetitive or microhomologous DNA
285 (*CLASP2*) (**Fig. 4o**). Each of these features has a high positive correlation (Pearson corr. >
286 0.93) with the number of deletions in repetitive DNA. This correlation suggests that all eight
287 models relate to a genome-instability phenotype, which may be driven by the *MSH3* co-mutated
288 tumours or, potentially, a concurrent deficiency of other genes within the mismatch repair
289 system (**Additional file 1, Supplementary Table 9**). Notably, the deficiency models of *UBR5,*
290 *BMPR2, CLASP2,* and *SMC6* all had PR-AUC-E above 0.2 in the other data set, suggesting
291 that these genes are associated with the mismatch repair phenotype regardless of metastatic
292 state (**Supplementary Table 7**).
293
294 **Biallelic LOF of *MSH6* associated with increased number of deletions in repetitive DNA in**
295 **prostate cancer**
296 *MSH6*, a gene implicated in mismatch repair and microsatellite stability[14]**,** was mutated in both
297 alleles in 7 out of 342 HMF prostate cancer patients. We observed pathogenic indels in *MSH6* in
298 all 7 tumours, but only one of these in mono- or dinucleotide repeat DNA. *MSH6* deficiency
299 could be predicted with high accuracy (PR-AUC-E=0.25; AUROC=0.98) by an enrichment of
300 deletions in repetitive DNA (**Fig. 5a,b; Additional file 1, Supplementary Table 7**). This is
301 consistent with existing findings of mismatch repair deficiency and its presence in metastatic
302 prostate cancers[31].
303
304 **High predictive power for *CDK12* deficiency**
305 *CDK12* encodes a kinase that regulates transcriptional and post-transcriptional processes of the
306 DDR[32–34]. We found that *CDK12*-d prostate cancers had an increased number of mid- and large-
307 sized tandem duplications 100Kb - 10Mb, compared to CDK12-WT (**Fig. 5c,d**). Several studies
308 have observed similar tandem duplication phenotypes in ovarian cancers [17,18,35] and castration

309 resistant prostate cancers[36,37]. In agreement, nine of the ten patients in our data set were
310 treated with drugs associated with castration resistance (4 Enzalutamide, 3 Abiraterone, 1
311 Cabazitaxel,1 Pembrolizumab)[38].
312
313 Whereas the tandem duplication phenotype has been previously associated with loss of *CDK12*,
314 in this study we present the first predictive algorithm utilising and quantifying the high predictive
315 value of these patterns (PR-AUC-E=0.73 and AUROC=0.97). Indeed, the loss of CDK12 has
316 been demonstrated to sensitise cancer cells to CHK1-[7] and PARP-inhibitors[39,40].
317
318 We went on to test the *CDK12*-d model across other cancer types (**Fig. 5c**). As expected, we
319 observed predictive power in cancers of the ovary and breast, though at a lower level (PR-AUC-
320 E=0.19 and AUROC=0.72). No predictive power was observed for the remaining cancer types.
321 We only observed a single tumour with ballelic LOF of *CDK12* in PCAWG, but the predictive
322 model was able to correctly identify this tumour, and reached a PR-AUC-E of 0.99 in the
323 PCAWG data set.
324
325 **Novel predictive gene deficiency models**
326 The shortlisted predictive LOF models further include biallelic LOF of *ATRX, PTEN, HERC2,*
327 *MEN1, SMARCA4, BAP1,* and *RB1,* as well as monoallelic LOF of *ATRX, IDH1, PTEN,*
328 *CDKN2A, ARID1A, TP53BP1, HERC2,* and *RB1* (**Fig. 3e; Additional file 1, Supplementary**
329 **Table 7)**. The number of mutated tumours underlying each model varied from eight (biallelic
330 *SMARCA*-d in cancers of unknown primary) to 22 (monoallelic *HERC2*-d in skin). We here
331 present the models of *ATRX, IDH1, SMARCA4, CDKN2A, PTEN, and HERC2*; remaining
332 models may be found in the supplementary material (**Additional file 1, 3, 4, Supplementary**
333 **Table 7, Supplementary Fig. 1**).

334

335 **Predictive models of *ATRX*-d and *IDH1*-d in CNS cancers**

336 We found that *ATRX*-d (monoallelic: PR-AUC-E=0.21, AUROC=0.71; biallelic: PR-AUC-E=0.23,
337 AUROC=0.76; **Fig. 6a**) and *IDH1*-d (monoallelic: PR-AUC-E=0.24, AUROC=0.82; **Fig. 6b**) in
338 CNS cancers were both predicted by a decreased number of SBS signature 8 mutations. In
339 addition, *ATRX*-d was further predicted by non-clustered inv. 10-100Kb, although with a small
340 coefficient and hence contributing limited discriminatory power. We discovered that 7 of11 *IDH1*
341 mutated tumours were also *ATRX* mutated (28-fold enrichment compared to *IDH1* WT skin
342 cancers; $p=1.2x10^{-8}$, Fisher's exact test) and that both *ATRX* and *IDH1* were predominantly hit
343 by somatic mutations (14 of 15 for *ATRX*, 11 of 11 for *IDH1*).

344

345 Co-mutation between *IDH1* and *ATRX* is well-described in gliomas[41]. Interestingly, LOF of either
346 gene is associated with lack of SBS signature 8, a signature associated with BRCAness[9,42] and
347 late-replication errors[43]. This suggests that CNS cancers with *IDH1/ATRX* deficiency are not
348 subject to the same DNA lesions or repair processes as other CNS cancers and they may
349 potentially belong to a separate patient subclass, though we could not identify evidence of this.

350

351 **Predictive model for *SMARCA4*-d in cancer of unknown primary**

352 We discovered eight tumours (HMF) out of 77 with cancers of unknown primary with
353 *SMARCA4*-d (biallelic) that could be predicted with relatively high accuracy (PR-AUC-E=0.44;
354 AUROC=0.85; **Fig. 6c**). These tumours showed an enrichment of SBS signature 27 (a signature
355 first detected in myeloid cancers [44]), which has been suggested to be a sequencing artefact
356 though it also displays strong strand bias [21] (**Additional file 1, Supplementary Table 5**).
357 Among cancers of unknown primary, SBS signature 27 correlates strongly with SBS signature 4
358 (Pearson corr.=0.96), despite the signatures different composition (cosine similarity of

359 signatures = 0.17) (**Additional file 1, Supplementary Table 9; Fig. 6h,i**). This suggests that
360 SBS signature 4 may also be associated with *SMARCA4*-d and we indeed found that its
361 predictive performance (PR-AUC-E of 0.43; AUROC=0.83) was almost equivalent to SBS
362 signature 27. Signature 4 is associated with smoking across several cancer types[45,46];
363 interestingly, *SMARCA4*-d is seen in aggressive thoracic sarcomas[47] and strongly enriched
364 among patients with a history of smoking[48]. Its gene product, BRG1, has been suggested as a
365 lung cancer transcriptional regulator of genes that induce tumour proliferation[49] and
366 metastasis[50]. We evaluated the ability of SBS signature 4 to predict *SMARCA4*-d in other
367 cancer types and found a significant predictive association in lung cancer, though much lower
368 than for cancers of unknown primary (**Fig. 6j**). We also found a significant ability to predict
369 *SMARCA4*-d by the number of SBS signature 27 mutations in cancers of the NET (Wilcoxon
370 test, one-tailed p=0.002) and head and neck ($p=4.8x10^{-7}$), but we could not evaluate this in lung
371 cancers, as the signature is not among its set of cohort-specific signatures.
372
373 Twelve cancers had a high posterior probability of *SMARCA4*-d (**Fig. 6j**) despite being
374 *SMARCA4* WT and lacking pathogenic events. No other single DDR gene was mutated among
375 all twelve tumours, with *TP53* having the most LOF events (6 of 12 cancers). Given that cancers
376 of unknown primary have disparate origins, this raises the possibility that the patients with high
377 posterior probability of *SMARCA4*-d may have metastasized from a cancer type or subtype with
378 both high levels of SBS signature 4 and 27, as well as high incidence of *SMARCA4*-d. Further
379 studies are thus needed to clarify if the observed associations can be explained through such
380 an ascertainment bias rather than causatively by *SMARCA4*-d.
381
382 **Predictive model for monoallelic *CDKN2A*-d in skin cancer**
383 Both germline and somatic variants in *CDKN2A* are known to predispose for melanoma[51]. In the

384 PCAWG skin cancer cohort, we found that a monoallelic predictive model of *CDKN2A*-d
385 achieved relatively high accuracy (PR-AUC-E=0.28; AUROC=0.82). Its predictive features are
386 enrichment of deletions at sites of microhomology, non-clustered inv. (100Kb-1Mb), and SBS
387 signature 7, in order of predictive importance (**Fig. 6d**). Apart from the inversions, these features
388 are also significantly associated with biallelic *CDKN2A*-d in the HMF skin cancer cohort
389 (**Additional file 4, Supplementary Fig. 2a,b**) and are included in the corresponding predictive
390 model, though it had lower predictive performance (PR-AUC-E=0.008; AUROC=0.542) and was
391 not shortlisted (**Additional file 1, Supplementary Table 6**). In both HMF and PCAWG, most of
392 the observed LOF events are somatic, with the majority being biallelic (16 of 18 in PCAWG; 32
393 of 33 in HMF; **Additional file 1, Supplementary Table 8**). The presence of deletions at sites of
394 microhomology suggests a possible reduction in error-free double-stranded break repair in
395 combination with an increased accumulation of SBS signature 7.
396
397 **Predictive model for *HERC2-d* in metastatic skin cancer**
398 *HERC2*-d has been associated with susceptibility to developing melanoma[52]. We found *HERC2*-
399 d predictable in HMF skin cancer patients (biallelic: PR-AUC-E=0.24, AUROC=0.73;
400 monoallelic: PR-AUC-E=0.23, AUROC=0.66; **Fig. 6e)**, primarily based on enrichment of
401 deletions in non-microhomologous and non-repetitive regions.
402
403 *HERC2* encodes a protein ligase that modulates the activity of P53[53]. We observed that seven
404 of the nine tumours with biallelic *HERC2*-d also had a monoallelic pathogenic event in *TP53* (8-
405 fold enrichment; $p=4.6x10^{-6}$, Fisher's exact test). Tumours that are co-mutated in *TP53*
406 (monoallelic) and *HERC2* (mono- or biallelic) showed a significantly higher number of deletions
407 compared to tumours with LOF in either gene alone (Wilcoxon test, One-tailed $p<0.031$) and

408 cancers that are wild-type for both genes ($p<7.2x10^{-7}$) (**Additional file 4, Supplementary Fig.**
409 **2c**).
410
411 ***PTEN* deficiency associates with fewer structural variants in CNS and uterine cancers**
412 *PTEN* is a tumour suppressor gene found in various cancer types[54,55] and its deficiency was
413 found to be associated with mutational patterns in uterine and CNS cancers (**Additional file 1,**
414 **Supplementary Table 7**). In CNS, we acquired two identical models from the HMF data set, as
415 we observed no monoallelic events without a second hit (mono- and biallelic PR-AUC-E=0.37,
416 AUROC=0.74; **Fig. 6f**). In uterine cancer, we acquired significant predictive models from both
417 HMF and PCAWG (HMF, biallelic: PR-AUC-E=0.37, AUROC=0.74; HMF, monoallelic: PR-AUC-
418 E=0.36, AUROC=0.79; PCAWG, monoallelic: PR-AUC-E=0.22, AUROC=0.74; **Fig. 6g**). In
419 addition, the models of *PTEN* loss in uterus had predictive power in the other data sets,
420 suggesting signal robustness and independence of metastatic state (the PCAWG derived model
421 had PR-AUC-E of 0.55 in the HMF data; the HMF derived model had a PR-AUC-E of 0.27 in
422 PCAWG; **Supplementary Table 7**). The model of biallelic *PTEN*-d in uterine cancers is
423 primarily based on depletion of non-clustered inv. 10-100Kb, whereas both the HMF and
424 PCAWG models of monoallelic deficiency are primarily based on depletion of non-clustered
425 tandem duplications (10-100Kb) (**Fig. 6g**). In contrast, our models of *PTEN*-d in CNS cancers
426 from HMF were based on depletion of both non-clustered deletions 1-10Kb and non-clustered
427 translocations (**Fig. 6f**).
428
429 **DISCUSSION**
430 The cancer-specific, incomplete repair of endogenous and exogenous DNA lesions leave
431 specific genome-wide mutational patterns. Their detection provides potentially powerful
432 information on the fidelity of individual DNA repair pathways and response to chemo- and

433 immunotherapies. Taking advantage of a large pan-cancer data set, our analysis shows that
434 mutational patterns are associated with DNA repair defects across a wide range of cancers and
435 repair mechanisms. In this study, we have contributed concrete initial predictive algorithms for
436 mutational patterns of several DDR gene deficiencies, with potential use for clinical intervention.
437
438 The clinical scope of our approach is exemplified by recent regulatory approval for PARPi
439 administration, which was supported by statistical predictions of homologous recombination
440 deficiency (HRD) based on mutational patterns[56] We have similarly predicted *CDK12* deficiency
441 (*CDK12*-d) which has previously been associated with a tandem duplication phenotype– with
442 power similar to that of HRD detection. This suggests a clinical benefit of clinical application of
443 predictive algorithms to test for *CDK12*-d, specifically when considering the application of
444 CHK1-inhibitors in prostate, ovary, and breast cancer treatment[7].
445
446 We also find high predictive power for *MSH6*-d in prostate cancers by counting deletions in
447 repetitive DNA, also known as the microsatellite instability phenotype (MSI)[57]. It is common
448 practice to search for signs of MSI in colorectal cancers, endometrial cancers, and aggressive
449 prostate cancers. This prediction is most commonly made using a panel of repetitive DNA
450 regions, such as the Bethesda panel[58]. Here we demonstrated high predictive power in prostate
451 cancers based on mutation summary statistics, which may be routinely extracted from whole
452 genome sequencing. The correct identification of tumours with high MSI supports the
453 administration of immune checkpoint blockade treatment, as the mutational phenotype leads to
454 an increased expression of neo-peptides and thus an increased sensitivity towards the immune
455 response[59,60].
456

457 Our systematic approach identified a similar model of *PTEN* LOF in uterine cancer in the
458 PCAWG data and the HMF data; either model also having predictive power in the other data
459 set. The re-discovery in either dataset grants further trust to this model, and further experimental
460 investigation is warranted to understand the underlying aetiology of the mutation patterns, and
461 the potential for clinical benefits.
462
463 Recent studies have suggested the use of CDK4/6 inhibition in treating *SMARCA4* deficient
464 tumours[61]. We discovered that a large subset of cancers of unknown primary (>10%) have
465 *SMARCA4* deficiency and that these cancers can be accurately predicted from their whole
466 genome accumulation of SBS signature 4 or SBS signature 27 mutations. This is a clinically
467 challenging cancer type due to the lack of a primary cancer to guide treatment and any such
468 prediction may serve in selecting treatment for these complex cancers, given additional
469 experimental evaluation.
470
471 Of note, the inclusion of monoallelic events allowed for larger sets of tumours with DRR gene
472 LOF, thereby increasing the power of our study when causative associations with mutational
473 patterns exist. This is for instance the case for *TP53,* which is known to be functionally impacted
474 by monoallelic events[62]. We shortlisted 11 models of TP53-d, which were all monoallelic. We
475 further found that inclusion of monoallelic LOF events matched the predictive power for *ATRX*
476 biallelic LOF in CNS cancers and *HERC2* biallelic LOF in skin cancers, suggesting that single
477 genetic hits are sufficient to affect repair and ensuing mutational patterns for these genes.
478
479 Incorrectly annotated LOF events in DDR genes may affect both the ability to discover
480 associations with mutational patterns and the performance of any associated predictive models.
481 On the other hand, highly stringent LOF criteria may result in true LOF events being overlooked,

482 and create small deficiency sets with insufficient power to discover true associations. For the
483 annotation of germline LOF events, we restricted our focus to rare variants (population
484 frequency ≤0.5%), as more common variants are likely benign. Given the high number of
485 variants evaluated overall, false positive germline LOF calls are expected. However, they are
486 unlikely to associate with specific mutational patterns and thus are unlikely to contribute
487 significant, shortlisted false positive predictive models of DDR deficiency. Likewise, in cancers
488 with hypermutator phenotypes, somatic LOF events may be caused by and associated with
489 specific mutational patterns. This leads to predictive models that in effect detect instances of
490 reverse causality, as discussed for the monoallelic models found in colorectal cancer. We
491 investigated whether reverse causality was a likely explanation for an association captured by a
492 predictive model by evaluating whether the annotated LOF events matched the predictive
493 mutational features (**Additional file 1, Supplementary Table 9**). In general, biallelic LOF
494 criteria is less sensitive to wrongly annotated LOF events than monoallelic criteria, as double
495 hits are rare compared to single hits. For both mono- and biallelic predictive models, the data
496 permutations ensure that the observed association between the DDR gene LOF events and
497 given mutational patterns are surprising.
498
499 Our conservative LOF curation, and a lack of expression or protein level data, is expected to
500 cause some LOF events to be missed. This may explain a high posterior probability of a
501 particular gene LOF in some tumours, but no evidence of genetic disruption (as seen in **Figure**
502 **5e** and **Figure 6h**). This highlights the scope of mutation-pattern-based predictions, in particular
503 in tumours without canonical DDR gene LOF events. At a very least, such tumours could be
504 considered for further scrutiny for LOF of the individual DDR gene that they are predicted to
505 have lost.
506

507 Our systematic approach provides a proof-of-concept that will become increasingly powerful as
508 the available data sets increase in number and size. For the current data sets, consistent
509 validation of detected associations was challenging due to small cohorts and differences in
510 cancer biology. To establish the basis for any future synthetic-lethality uses of our predictive
511 models, it would be desirable to establish causal relationships. This has been beyond the scope
512 of this study but could be achieved by whole-genome-sequencing of cell-lines or organoids with
513 individual DDR gene knockout. Alternatively, the loss of DDR genes can be explored in animal
514 models as previously done for several DDR genes including *BRCA1/2*[63], MMR genes[64,65], and
515 *TP53*[66].
516
517 The current study yields a catalogue of predictive models that captures both known and novel
518 associations between DDR gene deficiencies and mutational patterns. The included DDR genes
519 may provide targets for research and development of treatment. With further optimization,
520 predictive models such as these may guide the selection of therapy by adding certainty of
521 disabled or compromised repair deficiency phenotypes found in cancers of individual patients.
522

523 **Materials and methods**

524 **Data**

525 The analysis was conducted on 6,098 whole cancer genomes and included a set of 6,065 whole
526 cancer genomes after filtering (see below). The data came from two independent data sets: the
527 Pan-Cancer analysis of Whole Genomes (PCAWG; tumours = 2,583; ICGC study ID.
528 EGAS00001001692)[19] and the Hartwig Medical Foundation (HMF; tumours = 3,515; Acc. Nr.
529 DR-044)[20]. The data sets contain tumours from 32 cancer types and represent diverse patient
530 groups in terms of age, gender, and disease history. PCAWG consists of tumours both with and
531 without metastasis, whereas HMF exclusively consists of donors with tumours showing

532 metastatic capability. To best relate the two data sets, all tumours are catalogued by the site of
533 primary disease. For 77 of the metastatic HMF tumours, the primary site was unknown, and
534 these are annotated as such (**Figure 1a; Additional file 1, Supplementary Table 1**).
535
536 **Curating samples**
537 In the HMF data, we selected the earliest available sample whenever multiple samples existed
538 for the same patient. For the PCAWG data, we used the official whitelist, obtained at the ICGC
539 resources (https://dcc.icgc.org/pcawg), and for patients with more than one sample, we always
540 selected the earliest, whitelisted sample available. We discarded six PCAWG samples of
541 bone/soft tissue, as these were discarded in prior publications based on the PCAWG data set[27]
542 leaving 2,568 PCAWG samples and 3,497 HMF samples across 32 sites of the body. A list of all
543 Donor IDs, Sample IDs, and primary sites of disease may be found in **Additional file 1,**
544 **Supplementary Table 1**.
545
546 **Curating variants for loss-of-function annotation**
547 We annotated variants across a set of 736 genes related to the DNA damage response
548 (**Additional file 1, Supplementary Table 2**). The set of genes is combined from three sources,
549 Knijnenburg *et al*.[24]; Pearl *et al*.[23]; and Olivieri *et al*.[25].
550
551 We filtered the downloaded variant call files (VCF) of all samples for variants between the
552 Ensembl (GRCH37/hg19) start- and end position of each DDR gene (see coordinates in
553 **Additional file 1, Supplementary Table 2**). We included variants classified as PASS in the
554 VCF files and variants of the PCAWG data set supported by at least two of our four variant
555 callers. Furthermore, we discarded all variants which occurred in more than 200 samples across
556 the two data sets in order to avoid noise arising from single nucleotide polymorphisms (SNPs)

557 called as single nucleotide variants (SNVs), SNPs with high frequency in particular populations
558 and possibly technical artefacts. We also discarded somatic variants with variant allele fractions
559 (VAF) below 0.2 and variants where gnomAD (V2.1.1) showed a germline population frequency
560 above 0.5%[67].
561
562 **Annotating pathogenic variants and mutations**
563 We annotated all variants and mutations with CADD phred scores (V1.6) in order to separate
564 likely pathogenic variants from likely benign variants[26]. All variants with CADD phred scores of
565 25 or higher were considered pathogenic, whereas non-synonymous mutations with CADD
566 phred scores below 25 and above 10 were considered variants of unknown significance (VUS).
567 Variants with CADD phred scores below 10 were considered benign. A CADD phred score of 25
568 is a conservative threshold[68], and only includes the 0.3% most-likely pathogenic variants. In
569 addition, we annotated all variants with their status in the ClinVar database (when present).
570 Combining ClinVar and CADD phred scores ensured that we would be able to discover
571 associations across all DDR genes, not only genes with ClinVar annotations, which are
572 expected to be incomplete for any given gene.
573
574 **Annotating loss of heterozygosity and deep deletions**
575 We also used the copy number profiles of each sample to discover genes with biallelic or
576 monoallelic losses of parts of genes. Any overlap between a gene and a copy number loss was
577 indicated as a loss-of-function event, under the assumption that losing any part of the protein
578 coding DNA is detrimental to the complete protein product. We considered events in which the
579 minor allele copy number was below 0.2 to be a loss of heterozygosity (LOH), whereas we
580 considered events with a total tumour copy number below 0.3 (major and minor allele
581 summarised) as deep deletions. This cutoff is adapted from the work of Nguyen *et al*.[10].

582

583 **Annotating biallelic and monoallelic gene hits**

584 We considered genes with a single pathogenic variant, either somatic or germline, to be
585 monoallelic hit (n = 25,399). In cases where the monoallelic hit is accompanied by a LOH, we
586 considered the event a biallelic loss (n = 6,640). Finally, genes that were completely depleted in
587 a sample were considered biallelic lost (n = 66). We did not consider a single LOH event as a
588 monoallelic loss due to the broad impact and high frequency of such events, with ~25 times
589 higher rates of LOH than deep deletions (**Figure 1b,c**).

590

591 **Mutational patterns of single base substitutions, indels and structural variants**

592 We summarised the genome-wide set of somatic mutations by using Signature Tools Lib,
593 developed by Degaspari *et al.*[27] Firstly, we used Signature Tools Lib to count single nucleotide
594 variants by base change and context, and assigned these counts to a set of organ-specific
595 signatures, as recommended by Degaspari *et al*. We then have converted the organ-specific
596 signature exposures to reference signature exposures using the conversion matrix found in the
597 supplementary material of the paper by Degaspari *et al.*[27] For twelve signatures (N1-N12) this
598 was not possible, and these signatures are considered to be novel. Likewise, two signatures
599 associated with mismatch repair (MMR) deficiency, MMR1 and MMR2, are associated with
600 several of the COSMIC MMR signatures. For these, we preserved the signature label as given
601 by Signature Tools Lib. For cohorts with no organ-specific signatures (cancers of unknown
602 primary, neuroendocrine tissue, thymus, urinary tract, penis, testis, small intestine, vulva, double
603 primary, and the adrenal gland), we have assigned mutations directly to the full set of 30
604 reference signatures (COSMIC signatures 1-30). Note that we excluded age-related signature 1
605 from the modelling, as this signature confounded by acting as a proxy for the age of the patient

606 so that the model would be learning to differentiate old from young patients rather than patients
607 with activity of different mutational processes or repair deficiencies.
608
609 Secondly, Signature Tools Lib was used to count indels: insertions were simply counted,
610 whereas deletions were separated by the DNA context of the deletion, being microhomologous,
611 repetitive, or none of the two. Microhomology was defined by whether the deleted sequence
612 was similar to the region immediately 3' of the breakpoint, as this indicates repair by
613 microhomology-mediated end joining. Repetitive deletions were defined by whether there is a
614 repeat of the indel at the 3' end of the breakpoint[27]. We decided to not further compose indels
615 into signatures, for the ease of interpretation; the type of deletion has a clear relation to the
616 mechanism of repair, which is what we are investigating in this paper.
617
618 Finally, we used Signature Tools Lib to count structural variants. SVs were separated into two
619 groups, clustered and non-clustered based on the average distance between rearrangements
620 (the inter-rearrangement distance). Regions with at least 10 breakpoints having at least 10
621 times smaller inter-rearrangement distance than the average across the genome of that cancer,
622 were considered clusters[69]. SVs were further divided based on the type of mutation: Deletions,
623 tandem duplications, inversions, and translocations. Deletions, tandem duplications, and
624 inversions were further divided by size, with intervals being 1-10Kb, 10-100Kb, 100Kb - 1Mb, 1-
625 10Mb, and finally mutations with lengths above 10Mb. As with indels, we decided not to
626 decompose SV counts into rearrangement signatures, to ease interpretability and because SV
627 signatures are less established in the field. The per-sample exposure to each summary statistic
628 may be seen in **Additional file 1, Supplementary Table 3** (log transformed and scaled in
629 **Additional file 1, Supplementary Table 4;** see method below) and the suggested aetiology
630 (when existing) may be seen in **Additional file 1, Supplementary Table 5**[21,42].

631

632 **Preparing subsets of data for modelling**

633 We separated the two data sets and divided the tumours into their respective cancer-type
634 cohorts. We stratified the data for each DDR gene; designating whether the patient had a
635 biallelic pathogenic variant, monoallelic pathogenic variant, or no pathogenic variants. We
636 excluded tumours with inconclusive variants (CADD phred >10, <25) within the gene. For
637 modelling of cancers with biallelic variants in a gene, we selected all DDR gene-cohort
638 combinations where more than five tumours had biallelic variants in the same gene (n=194.
639 Likewise, we selected all cases with more than ten tumours with monoallelic variants (n = 341)
640 (**Additional file 1, Supplementary Table 6**). This setup means that each sample may be
641 included in developing several models but occur only once in each model as either mutated or
642 non-mutated. Biallelic mutated tumours were also included in the models of monoallelic loss, as
643 we consider biallelic loss a special case of monoallelic loss.

644

645 **Generating models using LASSO regression**

646 For each model we calculated per-sample weights to counter the imbalance in the data, so that
647 the weight of each sample was one minus the proportion of tumours with this mutational status
648 (either pathogenic or non-pahogenic/wildtype). We then used logistic regression model with
649 least absolute shrinkage and selection operator (LASSO) regularisation (henceforth LASSO
650 regression), with the alpha parameter at 1, from the R-package "glmnet" (v4.0)[70] to select
651 features with predictive power. The LASSO regression was selected to achieve a sparse set of
652 associated features that could be readily interpreted. This is in line with the methodology used in
653 HRDetect by Davies *et al.*[9].

654

655 For each of k cross-fold validation sets (with k being the number of biallelic or monoallelic hit
656 tumours, respectively), we ran a LASSO regression with a nested 5-fold cross-validation and the
657 assigned weights (as mentioned above to counter imbalance in the data), to produce a set of
658 lambda values. From the LASSO regression we selected the lambda value corresponding to the
659 binomial deviance which is one standard deviation away from the observed minimal binomial
660 deviance of the regression, in order to avoid overfitting (overfitting may occur if taking the
661 lambda of the minimal binomial deviance)[70]. In a few cases, the LASSO regression converged
662 to larger sets of features than what is justifiable by the low number of mutated tumours, and so
663 we limited the number of features to one feature per ten mutated tumours, rounded up and
664 added one (e.g. 12 mutated tumours gives basis for maximum three features). For each of the k
665 cross-folds we used the model to predict the left-out data and used these predictions for the
666 evaluation of the model performance.
667
668 Finally, we generated a model by including the entire data set. This was done to train the best
669 possible model in terms of selected features and coefficients, and this is the model reported in
670 the main figures, whereas the performance measures shown in the main figures are derived
671 from the k-fold cross-validation.
672
673 **Evaluating model predictive performance**
674 We used k-fold cross validation to get a measure of the predictive performance of each model.
675 Due to the strong imbalance in the data, we use the precision-recall area-under-the-curve (PR-
676 AUC) enrichment from the true-positive rate (PR-AUC-E) as our statistic of performance, while
677 also reporting traditional AUROC scores. The true-positive rate is the baseline that would be
678 expected for a non-informed model. By subtracting the true-positive rate from the PR-AUC of
679 each model, we can compare the performance between models despite different sample sizes.

680

681 **Model selection**

682 We selected models for further analysis (our shortlist) based on both their PR-AUC-E
683 performance (effect size) and their significance. Across the 535 initial models, we observed a
684 mean PR-AUC-E of 0.04 with a standard deviation of 0.099 (90%-quantile = 0.18) (**Additional**
685 **file 1, Supplementary Table 6**). The PR-AUC-E threshold was set at 0.2 and thus roughly two
686 standard deviations above the overall mean (**Additional file 1, Supplementary Table 7**).
687 To evaluate significance, we generated a null-distribution for each of the 535 initial models. This
688 was done by permuting the mutation state of the underlying tumours and then running the
689 LASSO regression on the permuted data. We ran a minimum of 10,000 permutations (n) for
690 each of the 535 models, storing the PR-AUC-E for each permutation. For models where the
691 number (r) of permutations leading to PR-AUC-E values as or more extreme than the original
692 model was smaller than five, we ran an additional 10,000 permutations, up to a maximum of
693 30,000 permutations. A p-value (p=$(r+1)/n$) was calculated for each model (**Additional file 1,**
694 **Supplementary Table 6**). The Benjamini-Hochberg procedure was used to control the false
695 discovery rate and resulting adjusted p-values (q-values) smaller than 0.05 were considered
696 significant (**Additional file 1, Supplementary Table 7**).

697

698 In conclusion, 48 models of 24 genes were shortlisted for further investigation. Of these, we
699 describe 43 in the main text and, more briefly, 5 in **Supplementary text** and **Supplementary**
700 **figure 1.** The inclusion into the main manuscript was done by collegial evaluation of interest to
701 the field and does not represent a definitive difference in quality of the models.

702

703 **DECLARATIONS**

704 **Ethics approval and consent to participate**

705 We analysed data generated and made available by the Pan-Cancer Analysis of Whole
706 Genomes (PCAWG)[19] Consortium of the International Cancer Genome Consortium (ICGC) and
707 The Cancer Genome Atlas (TCGA) as well as the Hartwig Medical Foundation[20]. The research
708 conforms to the principles of the Helsinki Declaration.
709
710 **Availability of Data and Materials**
711 The data sets supporting the conclusions of this article are from the Pan-Cancer Analysis of
712 Whole Genomes and from the Hartwig Medical Foundation. The public parts of the PCAWG
713 data set is available at https://dcc.icgc.org/releases/PCAWG, whereas controlled files may be
714 accessed through gbGaP and daco, as instructed on this site https://docs.icgc.org/pcawg/data/.
715 The ICGC study ID of the project is EGAS00001001692.
716
717 The HMF data used in this project may be found by accession code DR-044 and can be
718 obtained upon request at the Hartwig Medical Foundation
719 (https://www.hartwigmedicalfoundation.nl/en).
720
721 **Code availability**
722 The code needed to reproduce the analysis will be made available at
723 https://github.com/SimonGrund/DDR_Predict , including data pre-processing, modelling of the
724 535 predictive models and modelling of ≥10,000 data permutation null models for each of the
725 535 models.
726
727 **Competing interests**
728 The authors declare no competing interests.
729

Funding

ERH and AS were funded by the Novo Nordisk Foundation (NNF15OC0016662), Cancer Research UK (C23210/A7574), and the Danish National Research Foundation (Center grant, DNRF115). JSP, SGS, GAP, and MHC were funded by the Independent Research Fund Denmark | Medical Sciences (8021-00419B), the Danish Cancer Society (R307-A17932), Aarhus University Research Foundation (AUFF-E-2020-6-14), a PhD stipend from Aarhus University, and a stipend from Research Foundation of Central Region Denmark (A2972).

Author contributions

The project was conceived and designed by JSP and SGS, with early contributions by JB. The data analysis was carried out by SGS under supervision of JSP with input from MHC, including data preparation, exploratory analysis, and statistical modelling. SGS generated all figures and tables. SGS, AS, GAP, ERH, and JSP interpreted the results. SGS, ERH and JSP wrote the manuscript. All authors accepted the manuscript.

Acknowledgements

We thank the Pan-Cancer Analysis of Whole Genomes (PCAWG), The International Cancer Genome Consortium (ICGC), and The Cancer Genome Atlas (TCGA) for access to whole cancer genomes. We would also like to thank the Hartwig Medical Foundation (HMF) and the Center for Personalized Cancer Treatment (CPCT) for creating and providing access to metastatic whole cancer genome data. We thank Jenny Gruhn and Amy V. Kaucher for valuable comments on the manuscript. We thank Dr. Andrea Degaspari for aid in using Signature Tools Lib for summarising mutation patterns.

REFERENCE LIST

754 1. Lindahl, T. Instability and decay of the primary structure of DNA. *Nature* **362**, 709–715
755 (1993).
756 2. Nik-Zainal, S. *et al.* Mutational Processes Molding the Genomes of 21 Breast Cancers. *Cell*
757 vol. 149 979–993 (2012).
758 3. Volkova, N. V. *et al.* Mutational signatures are jointly shaped by DNA damage and repair.
759 *Nat. Commun.* **11**, 2169 (2020).
760 4. Bryant, H. E. *et al.* Specific killing of BRCA2-deficient tumours with inhibitors of poly(ADP-
761 ribose) polymerase. *Nature* vol. 447 346–346 (2007).
762 5. Le, D. T. *et al.* PD-1 Blockade in Tumors with Mismatch-Repair Deficiency. *N. Engl. J. Med.*
763 **372**, 2509–2520 (2015).
764 6. von Bueren, A. O. *et al.* Mismatch repair deficiency: a temozolomide resistance factor in
765 medulloblastoma cell lines that is uncommon in primary medulloblastoma tumours. *Br. J.*
766 *Cancer* **107**, 1399–1408 (2012).
767 7. Paculová, H. *et al.* BRCA1 or CDK12 loss sensitizes cells to CHK1 inhibitors. *Tumour Biol.*
768 **39**, 1010428317727479 (2017).
769 8. Landrum, M. J. *et al.* ClinVar: public archive of relationships among sequence variation and
770 human phenotype. *Nucleic Acids Res.* **42**, D980–5 (2014).
771 9. Davies, H. *et al.* HRDetect is a predictor of BRCA1 and BRCA2 deficiency based on
772 mutational signatures. *Nat. Med.* **23**, 517–525 (2017).
773 10. Nguyen, L., W M Martens, J., Van Hoeck, A. & Cuppen, E. Pan-cancer landscape of
774 homologous recombination deficiency. *Nat. Commun.* **11**, 5584 (2020).
775 11. McVey, M. & Lee, S. E. MMEJ repair of double-strand breaks (director's cut): deleted
776 sequences and alternative endings. *Trends Genet.* **24**, 529–538 (2008).
777 12. Nussenzweig, A. & Nussenzweig, M. C. A backup DNA repair pathway moves to the
778 forefront. *Cell* **131**, 223–225 (2007).

779 13. Umar, A. *et al.* Defective mismatch repair in extracts of colorectal and endometrial cancer
780 cell lines exhibiting microsatellite instability. *J. Biol. Chem.* **269**, 14367–14370 (1994).
781 14. Edelmann, W. *et al.* The DNA mismatch repair genes Msh3 and Msh6 cooperate in
782 intestinal tumor suppression. *Cancer Res.* **60**, 803–807 (2000).
783 15. Lanni, J. S. & Jacks, T. Characterization of the p53-dependent postmitotic checkpoint
784 following spindle disruption. *Mol. Cell. Biol.* **18**, 1055–1064 (1998).
785 16. Gorgoulis, V. G. *et al.* Activation of the DNA damage checkpoint and genomic instability in
786 human precancerous lesions. *Nature* **434**, 907–913 (2005).
787 17. Popova, T. *et al.* Ovarian Cancers Harboring Inactivating Mutations in CDK12 Display a
788 Distinct Genomic Instability Pattern Characterized by Large Tandem Duplications. *Cancer*
789 *Res.* **76**, 1882–1891 (2016).
790 18. Menghi, F. *et al.* The Tandem Duplicator Phenotype Is a Prevalent Genome-Wide Cancer
791 Configuration Driven by Distinct Gene Mutations. *Cancer Cell* **34**, 197–210.e5 (2018).
792 19. ICGC/TCGA Pan-Cancer Analysis of Whole Genomes Consortium. Pan-cancer analysis of
793 whole genomes. *Nature* **578**, 82–93 (2020).
794 20. Priestley, P. *et al.* Pan-cancer whole-genome analyses of metastatic solid tumours. *Nature*
795 **575**, 210–216 (2019).
796 21. Tate, J. G. *et al.* COSMIC: the Catalogue Of Somatic Mutations In Cancer. *Nucleic Acids*
797 *Res.* **47**, D941–D947 (2019).
798 22. Alexandrov, L. B. & Stratton, M. R. Mutational signatures: the patterns of somatic mutations
799 hidden in cancer genomes. *Curr. Opin. Genet. Dev.* **24**, 52–60 (2014).
800 23. Pearl, L. H., Schierz, A. C., Ward, S. E., Al-Lazikani, B. & Pearl, F. M. G. Therapeutic
801 opportunities within the DNA damage response. *Nat. Rev. Cancer* **15**, 166–180 (2015).
802 24. Knijnenburg, T. A. *et al.* Genomic and Molecular Landscape of DNA Damage Repair
803 Deficiency across The Cancer Genome Atlas. *Cell Rep.* **23**, 239–254.e6 (2018).

804 25. Olivieri, M. *et al.* A Genetic Map of the Response to DNA Damage in Human Cells. *Cell*
805 **182**, 481–496.e21 (2020).
806 26. Rentzsch, P., Witten, D., Cooper, G. M., Shendure, J. & Kircher, M. CADD: predicting the
807 deleteriousness of variants throughout the human genome. *Nucleic Acids Research* vol. 47
808 D886–D894 (2019).
809 27. Degasperi, A. *et al.* A practical framework and online tool for mutational signature analyses
810 show inter-tissue variation and driver dependencies. *Nat Cancer* **1**, 249–263 (2020).
811 28. Davis, J. & Goadrich, M. The relationship between Precision-Recall and ROC curves. in
812 *Proceedings of the 23rd international conference on Machine learning* 233–240
813 (Association for Computing Machinery, 2006).
814 29. Ceccaldi, R. *et al.* Homologous-recombination-deficient tumours are dependent on Polθ-
815 mediated repair. *Nature* **518**, 258–262 (2015).
816 30. Hanel, W. & Moll, U. M. Links between mutant p53 and genomic instability. *J. Cell.*
817 *Biochem.* **113**, 433–439 (2012).
818 31. Graham, L. S. *et al.* Mismatch repair deficiency in metastatic prostate cancer: Response to
819 PD-1 blockade and standard therapies. *PLoS One* **15**, e0233260 (2020).
820 32. Blazek, D. *et al.* The Cyclin K/Cdk12 complex maintains genomic stability via regulation of
821 expression of DNA damage response genes. *Genes Dev.* **25**, 2158–2172 (2011).
822 33. Marqués, F. *et al.* A new subfamily of high molecular mass CDC2-related kinases with
823 PITAI/VRE motifs. *Biochem. Biophys. Res. Commun.* **279**, 832–837 (2000).
824 34. Li, X., Chatterjee, N., Spirohn, K., Boutros, M. & Bohmann, D. Cdk12 Is A Gene-Selective
825 RNA Polymerase II Kinase That Regulates a Subset of the Transcriptome, Including Nrf2
826 Target Genes. *Sci. Rep.* **6**, 21455 (2016).
827 35. Li, Y. *et al.* Patterns of somatic structural variation in human cancer genomes. *Nature* **578**,
828 112–121 (2020).

829 36. Wu, Y.-M. *et al.* Inactivation of CDK12 Delineates a Distinct Immunogenic Class of
830 Advanced Prostate Cancer. *Cell* vol. 173 1770–1782.e14 (2018).
831 37. Rescigno, P. *et al.* Characterizing CDK12-Mutated Prostate Cancers. *Clinical cancer*
832 *research: an official journal of the American Association for Cancer Research* vol. 27 566–
833 574 (2021).
834 38. Sumanasuriya, S. & De Bono, J. Treatment of Advanced Prostate Cancer—A Review of
835 Current Therapies and Future Promise. *Cold Spring Harb. Perspect. Med.* **8**, (2018).
836 39. Bajrami, I. *et al.* Genome-wide profiling of genetic synthetic lethality identifies CDK12 as a
837 novel determinant of PARP1/2 inhibitor sensitivity. *Cancer Res.* **74**, 287–297 (2014).
838 40. Joshi, P. M., Sutor, S. L., Huntoon, C. J. & Karnitz, L. M. Ovarian cancer-associated
839 mutations disable catalytic activity of CDK12, a kinase that promotes homologous
840 recombination repair and resistance to cisplatin and poly(ADP-ribose) polymerase
841 inhibitors. *J. Biol. Chem.* **289**, 9247–9253 (2014).
842 41. Mukherjee, J. *et al.* Mutant IDH1 Cooperates with ATRX Loss to Drive the Alternative
843 Lengthening of Telomere Phenotype in Glioma. *Cancer Res.* **78**, 2966–2977 (2018).
844 42. Alexandrov, L. B. *et al.* The repertoire of mutational signatures in human cancer. *Nature*
845 **578**, 94–101 (2020).
846 43. Singh, V. K., Rastogi, A., Hu, X., Wang, Y. & De, S. Mutational signature SBS8
847 predominantly arises due to late replication errors in cancer. *Commun Biol* **3**, 421 (2020).
848 44. Alexandrov, L. B. *et al.* Clock-like mutational processes in human somatic cells. *Nat. Genet.*
849 **47**, 1402–1407 (2015).
850 45. Alexandrov, L. B. *et al.* Signatures of mutational processes in human cancer. *Nature* vol.
851 500 415–421 (2013).
852 46. Nik-Zainal, S. *et al.* The genome as a record of environmental exposure. *Mutagenesis*
853 gev073 (2015) doi:10.1093/mutage/gev073.

854 47. Sauter, J. L. *et al.* SMARCA4-deficient thoracic sarcoma: a distinctive clinicopathological
855 entity with undifferentiated rhabdoid morphology and aggressive behavior. *Mod. Pathol.* **30**,
856 1422–1432 (2017).
857 48. Rekhtman, N. *et al.* SMARCA4-Deficient Thoracic Sarcomatoid Tumors Represent
858 Primarily Smoking-Related Undifferentiated Carcinomas Rather Than Primary Thoracic
859 Sarcomas. *J. Thorac. Oncol.* **15**, 231–247 (2020).
860 49. Dagogo-Jack, I. *et al.* Clinicopathologic Characteristics of BRG1-Deficient NSCLC. *J.*
861 *Thorac. Oncol.* **15**, 766–776 (2020).
862 50. Concepcion, C. P. *et al.* SMARCA4 inactivation promotes lineage-specific transformation
863 and early metastatic features in the lung. *Cancer Discov.* (2021) doi:10.1158/2159-
864 8290.CD-21-0248.
865 51. Liu, L. *et al.* Mutation of the CDKN2A 5'UTR creates an aberrant initiation codon and
866 predisposes to melanoma. *Nat. Genet.* **21**, 128–132 (1999).
867 52. Amos, C. I. *et al.* Genome-wide association study identifies novel loci predisposing to
868 cutaneous melanoma. *Hum. Mol. Genet.* **20**, 5012–5023 (2011).
869 53. Cubillos-Rojas, M. *et al.* The E3 ubiquitin protein ligase HERC2 modulates the activity of
870 tumor protein p53 by regulating its oligomerization. *J. Biol. Chem.* **289**, 14782–14795
871 (2014).
872 54. Li, J. *et al.* PTEN, a putative protein tyrosine phosphatase gene mutated in human brain,
873 breast, and prostate cancer. *Science* **275**, 1943–1947 (1997).
874 55. Liaw, D. *et al.* Germline mutations of the PTEN gene in Cowden disease, an inherited
875 breast and thyroid cancer syndrome. *Nat. Genet.* **16**, 64–67 (1997).
876 56. Fda. FDA approves niraparib for HRD-positive advanced ovarian cancer. (2019).
877 57. Boland, C. R. & Goel, A. Microsatellite instability in colorectal cancer. *Gastroenterology*
878 **138**, 2073–2087.e3 (2010).

879 58. Umar, A. *et al.* Revised Bethesda Guidelines for hereditary nonpolyposis colorectal cancer
880 (Lynch syndrome) and microsatellite instability. *J. Natl. Cancer Inst.* **96**, 261–268 (2004).
881 59. Abida, W. *et al.* Analysis of the Prevalence of Microsatellite Instability in Prostate Cancer
882 and Response to Immune Checkpoint Blockade. *JAMA Oncol* **5**, 471–478 (2019).
883 60. Antonarakis, E. S. *et al.* Clinical Features and Therapeutic Outcomes in Men with
884 Advanced Prostate Cancer and DNA Mismatch Repair Gene Mutations. *Eur. Urol.* **75**, 378–
885 382 (2019).
886 61. Xue, Y. *et al.* SMARCA4 loss is synthetic lethal with CDK4/6 inhibition in non-small cell lung
887 cancer. *Nat. Commun.* **10**, 557 (2019).
888 62. Malcikova, J. *et al.* Monoallelic and biallelic inactivation of TP53 gene in chronic
889 lymphocytic leukemia: selection, impact on survival, and response to DNA damage. *Blood*
890 **114**, 5307–5314 (2009).
891 63. Evers, B. & Jonkers, J. Mouse models of BRCA1 and BRCA2 deficiency: past lessons,
892 current understanding and future prospects. *Oncogene* **25**, 5885–5897 (2006).
893 64. Reitmair, A. H. *et al.* MSH2 deficient mice are viable and susceptible to lymphoid tumours.
894 *Nat. Genet.* **11**, 64–70 (1995).
895 65. Prolla, T. A. *et al.* Tumour susceptibility and spontaneous mutation in mice deficient in
896 Mlh1, Pms1 and Pms2 DMA mismatch repair. *Nat. Genet.* **18**, 276–279 (1998).
897 66. Donehower, L. A. The p53-deficient mouse: a model for basic and applied cancer studies.
898 *Semin. Cancer Biol.* **7**, 269–278 (1996).
899 67. Karczewski, K. J. *et al.* The mutational constraint spectrum quantified from variation in
900 141,456 humans. *Nature* **581**, 434–443 (2020).
901 68. Itan, Y. *et al.* The mutation significance cutoff: gene-level thresholds for variant predictions.
902 *Nat. Methods* **13**, 109–110 (2016).
903 69. Nik-Zainal, S. *et al.* Landscape of somatic mutations in 560 breast cancer whole-genome

sequences. *Nature* **534**, 47–54 (2016).

70. Friedman, J., Hastie, T. & Tibshirani, R. Regularization paths for generalized linear models via coordinate descent. *J. Stat. Softw.* (2010).

908 **Figure titles and legends**

Figure 1

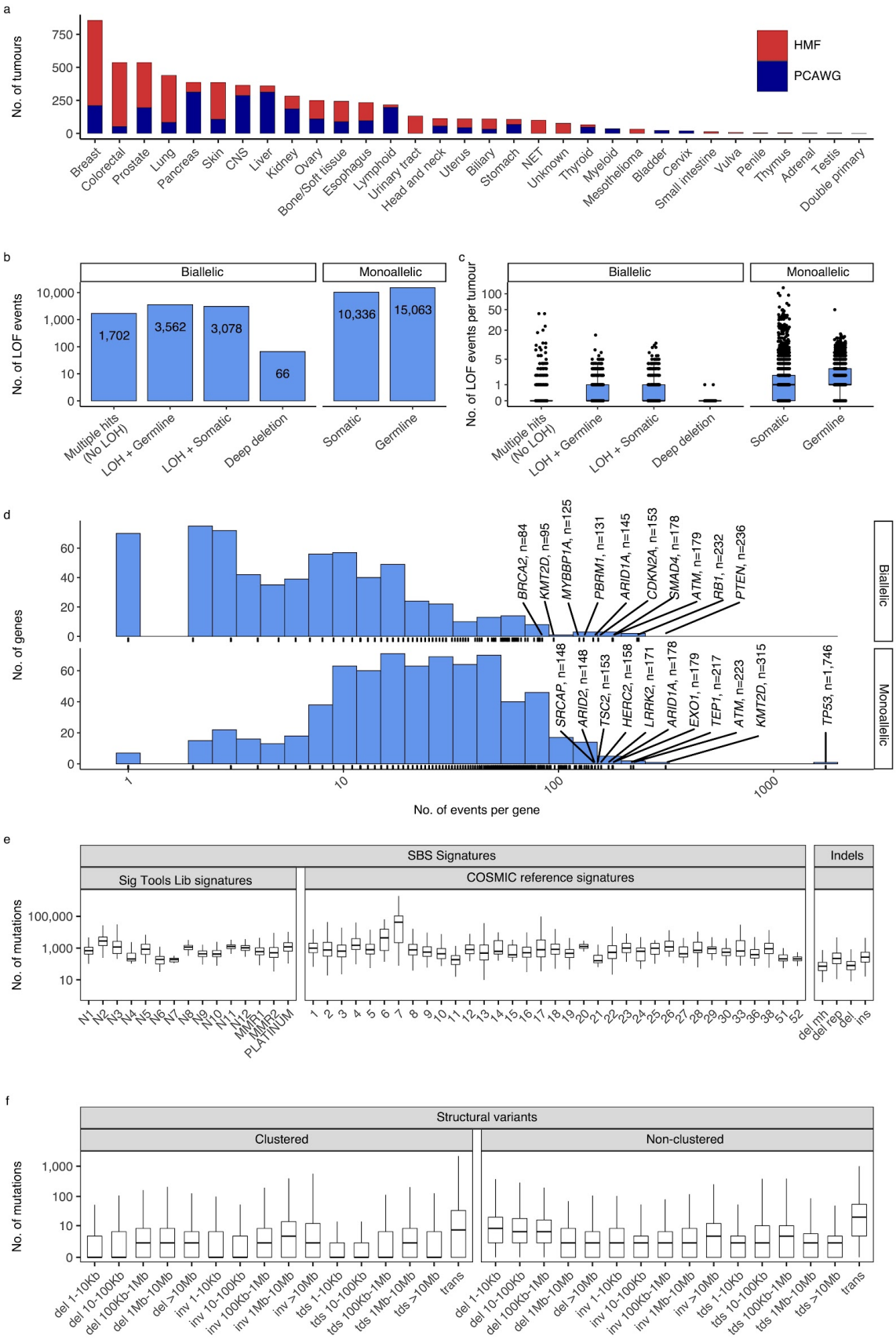
a
No. of tumours
HMF
PCAWG
Breast
Colorectal
Prostate
Lung
Pancreas
Skin
CNS
Liver
Kidney
Ovary
Bone/Soft tissue
Esophagus
Lymphoid
Urinary tract
Head and neck
Uterus
Biliary
Stomach
NET
Unknown
Thyroid
Myeloid
Mesothelioma
Bladder
Cervix
Small intestine
Vulva
Penile
Thymus
Adrenal
Testis
Double primary
b
No. of LOF events
Biallelic
Monoallelic
1,702
3,562
3,078
66
10,336
15,063
Multiple hits (No LOH)
LOH + Germline
LOH + Somatic
Deep deletion
Somatic
Germline
c
No. of LOF events per tumour
d
No. of genes
BRCA2, n=84
KMT2D, n=95
MYBBP1A, n=125
PBRM1, n=131
ARID1A, n=145
CDKN2A, n=153
SMAD4, n=178
ATM, n=179
RB1, n=232
PTEN, n=236
SRCAP, n=148
ARID2, n=148
TSC2, n=153
HERC2, n=158
LRRK2, n=171
ARID1A, n=178
EXO1, n=179
TEP1, n=217
ATM, n=223
KMT2D, n=315
TP53, n=1,746
No. of events per gene
e
No. of mutations
SBS Signatures
Sig Tools Lib signatures
COSMIC reference signatures
Indels
del mh
del rep
del
ins
f
Structural variants
Clustered
Non-clustered
del 1-10Kb
del 10-100Kb
del 100Kb-1Mb
del 1Mb-10Mb
del >10Mb
inv 1-10Kb
inv 10-100Kb
inv 100Kb-1Mb
inv 1Mb-10Mb
inv >10Mb
tds 1-10Kb
tds 10-100Kb
tds 100Kb-1Mb
tds 1Mb-10Mb
tds >10Mb
trans

910 **Figure 1: Cancer-types, DDR gene deficiencies, and mutational patterns**

911 **a** Cohort sizes for the 32 cancer types comprising the 6,065 whole cancer genomes collected
912 from the Hartwig Medical Foundation (HMF; n=3,497) and the PanCancer Analysis of Whole
913 Genomes (PCAWG; n=2,568). **b** mono- and biallelic loss-of-function (LOF) events were
914 annotated across 736 DDR genes based on both pathogenic variants and copy-number-losses
915 (loss of heterozygosity; LOH), overall and (**c**) per patient (**d**) with varying no. of LOF events per
916 DDR gene (x-axis; logarithmic). **e** Whole genome mutational patterns were represented as
917 summary statistics and used as input features for the predictive models of DDR gene deficiency.
918 Concretely, each patient was annotated with the number of single-base-substitutions (SBS) that
919 are accounted to each SBS signature (Alexandrov *et al.*[22]; Degaspari *et al*.[27]), number of indels
920 divided by context (mh = microhomology; rep = repetitive), and (**f**) number of structural variants
921 divided by clusterness, size, and type (del = deletion; inv = inversion; tds = tandem duplication;
922 trans = translocation)

923

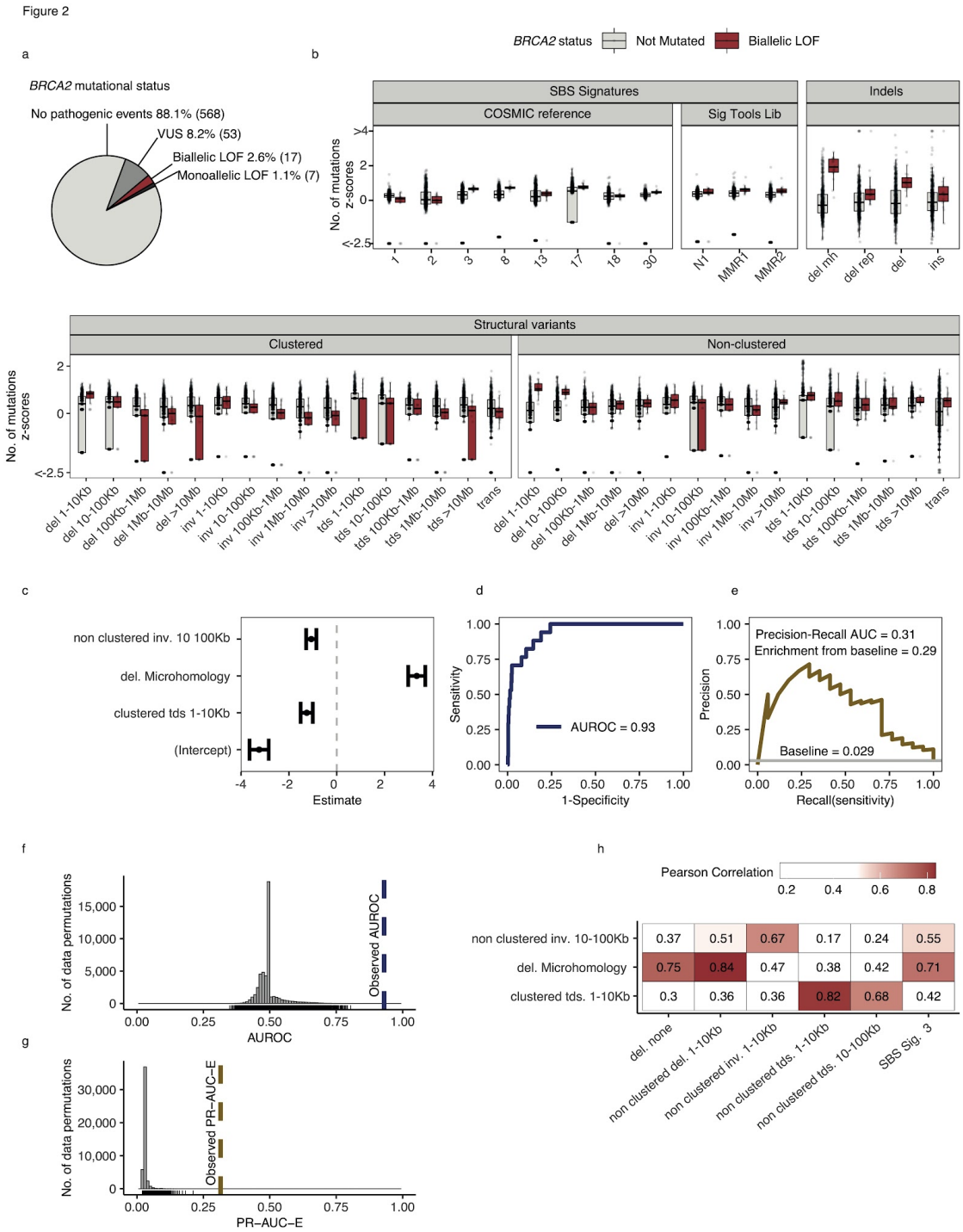

Figure 2: Predictive modelling of BRCA2 deficiencies in the HMF breast cancers

a Mutational status of *BRCA2* across 645 HMF breast cancer patients. **b** Mutational summary statistics for the HMF breast cancer patients divided by biallelic *BRCA2* loss-of-function (LOF;

red) and *BRCA2* wild type (WT; grey) (selected predictive features in bold). **c** Predictive features and their coefficients for model of biallelic *BRCA2* loss with predictive performance measured in (**d**) AUROC and (**e**) PR-AUC (PR-AUC-E=PR-AUC - baseline=0.29; **Methods**). **f** Distributions of AUROC and (**g**) PR-AUC-E values obtained from 30,000 random data permutations compared to observed values (punctuated lines). **h** Correlation between selected predictive features (horizontal) and other highly correlated (Pearson corr. >0.65) mutational features (vertical).

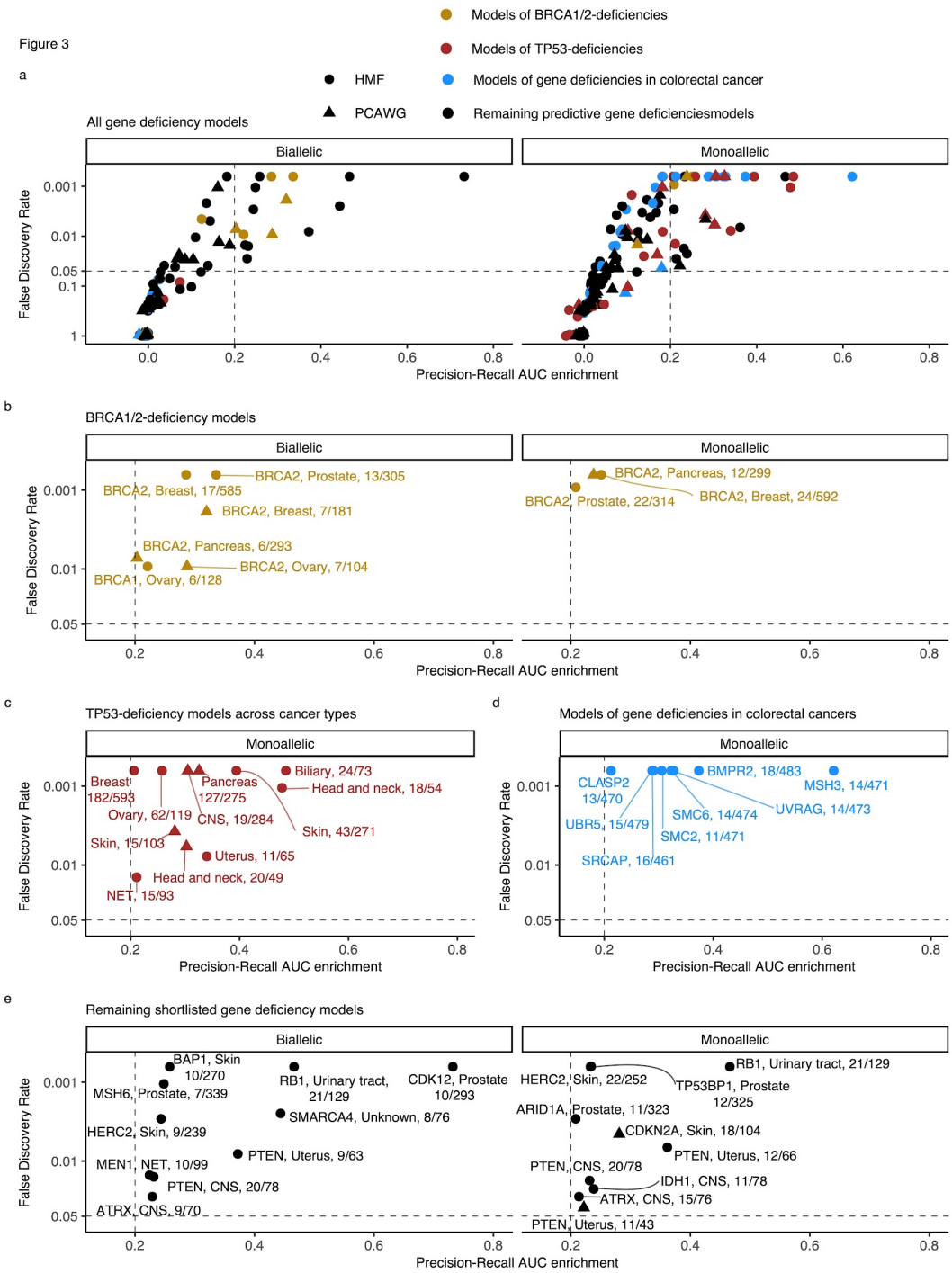

Figure 3: Predictive models of DDR gene deficiencies

a The precision-recall AUC enrichment PR-AUC-E; x-axis) and significance (FDR; logarithmic y-axis) of the 535 predictive models (one model per gene with more than five biallelic or more

939 than ten tumours either mono- or biallelic mutated in either HMF or PCAWG in any one cancer
940 type; **Methods**). Significance (q-value representing FDR) evaluated by counting equally or
941 more-extreme PR-AUC-E values across >10,000 permuted data sets and applying Benjamini-
942 Hochberg FDR control. Models with FDR below 0.05 and PR-AUC-E above 0.2 are shortlisted
943 (**Methods**). **b** Shortlisted predictive models of deficiency of *BRCA1* or *BRCA2*; (**c**) *TP53*
944 monoallelic predictive models; (**d**) monoallelic gene deficiency models across colorectal cancer
945 patients; (**e**) and remaining gene deficiency models not contained in the other sub-groups.
946 Numbers indicate the number of mutated out of the total number of tumours included in the
947 development of each model.
948

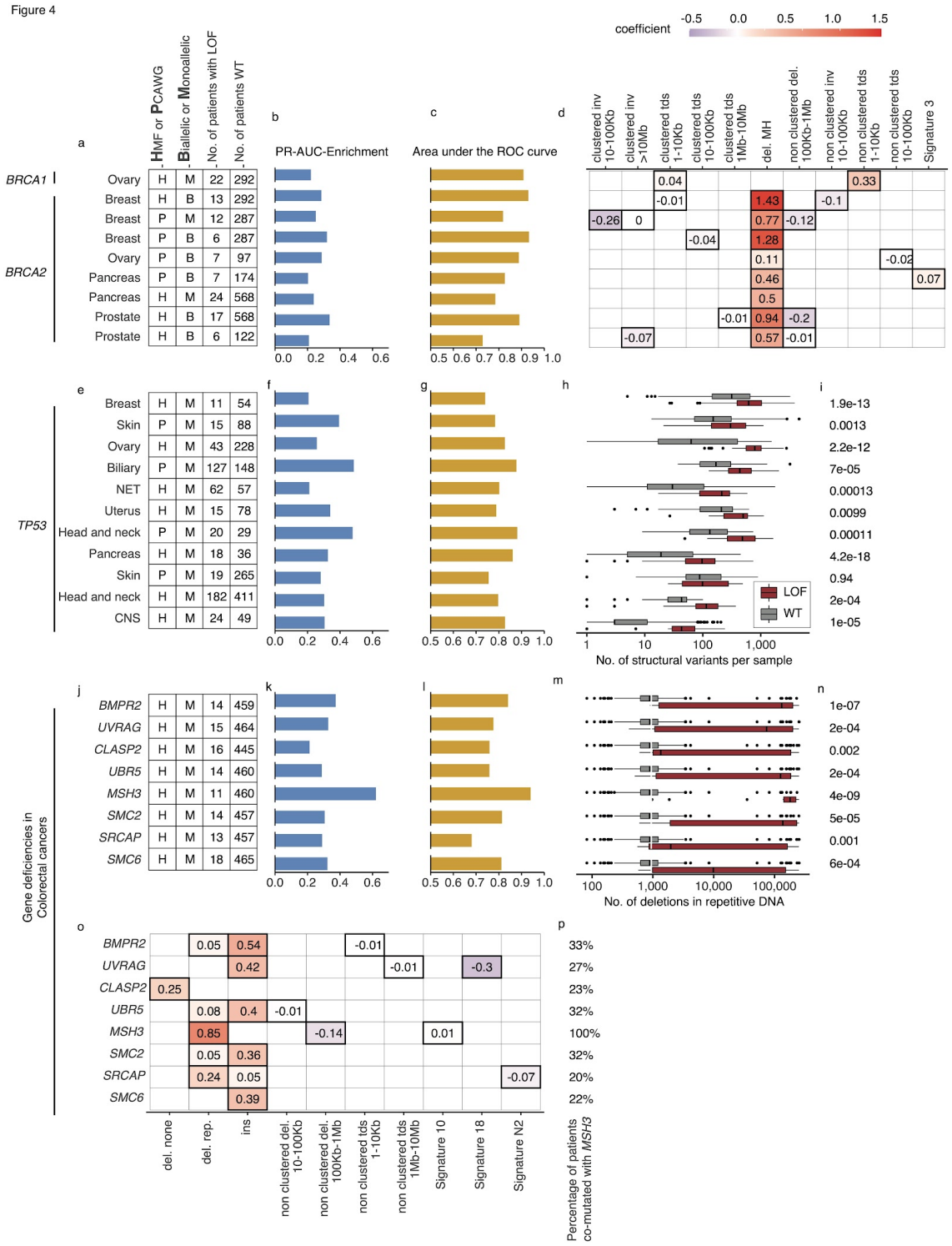

Figure 4: Predictive models with anticipated aetiology or origin

951 **a** Overview of predictive models for *BRCA1*-d and *BRCA2*-d, showing data source, type of
952 model, and LOF-set statistics *(***b**) PR-AUC-E, (**c**) AUROC, (**d**) and the predictive features and
953 their coefficient for individual models. **e,f,g** Overview of predictive models of *TP53*-d (as in a-c).
954 **h** For each cohort the number of structural variants (x-axis; logarithmic) for *TP53* LOF tumours
955 (red) versus *TP53* wild type tumours (grey) and (**i**) the significance of their difference (two-sided
956 Wilcoxon rank-sum test). **j,k,l** Predictive models of gene deficiencies in colorectal cancers (as in
957 a-c). **m** Number of deletions in repetitive DNA (as in h) and (**n**) its significance (as in i)**. o** The
958 predictive features of each model (as in d) and (**p**) the percentage of tumours that are co-
959 mutated with *MSH3*.
960

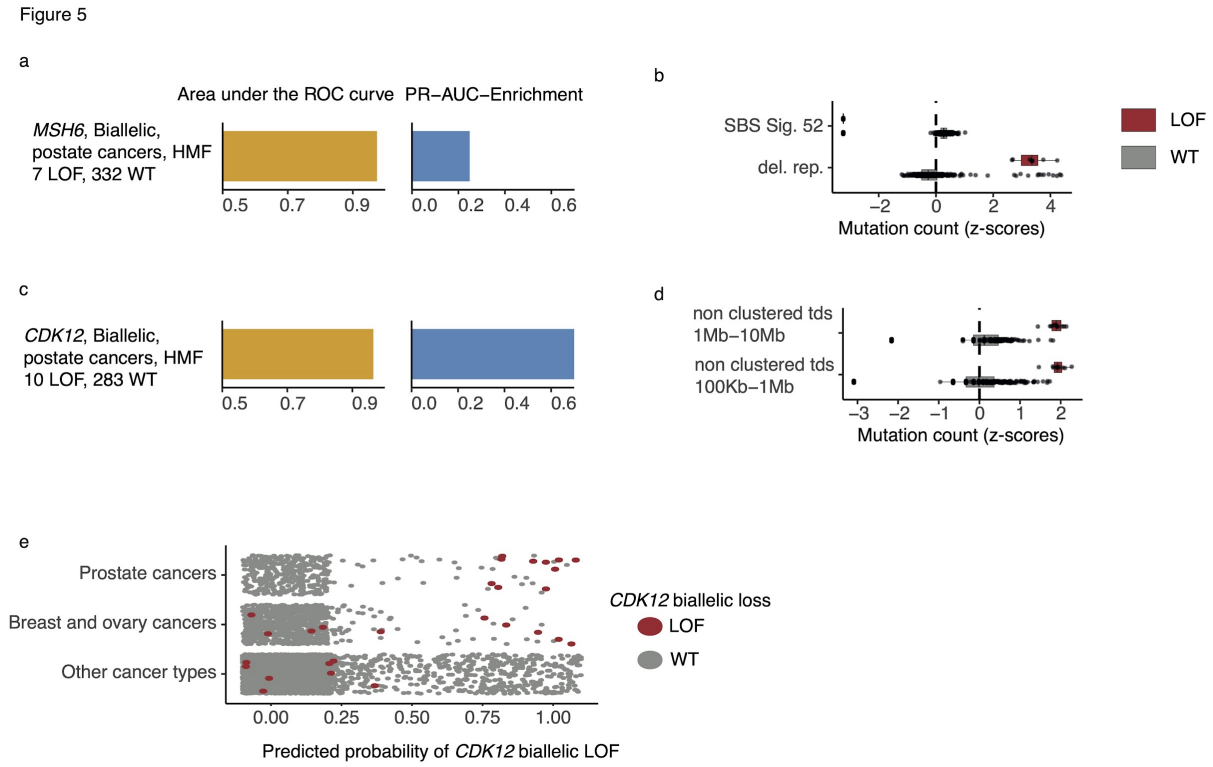

Figure 5: *CDK12* mutated prostate tumours are predicted by tandem duplications

a Biallelic predictive model *MSH6*-d in HMF prostate tumours and its PR-AUC-E and AUROC. **b** Boxplots of mutation counts between tumours that are *MSH6*-d loss-of-function (red) and *MSH6* wild-type (grey), (mutation counts are normalised and log-transformed; **Methods). c** Biallelic predictive model for *CDK12*-d with performance measures (as in a). **b** Boxplots of mutation counts for *CDK12* deficient and wildtype tumours (as in b). **e** *CDK12*-d predictive performance for different cancer types. Predicted probability of *CDK12*-d (x-axis) for tumours with *CDK12* LOF (red) and *CDK12* wild type (grey) are shown for prostate cancer, breast and ovary cancer, and all other cancer types (y-axis).

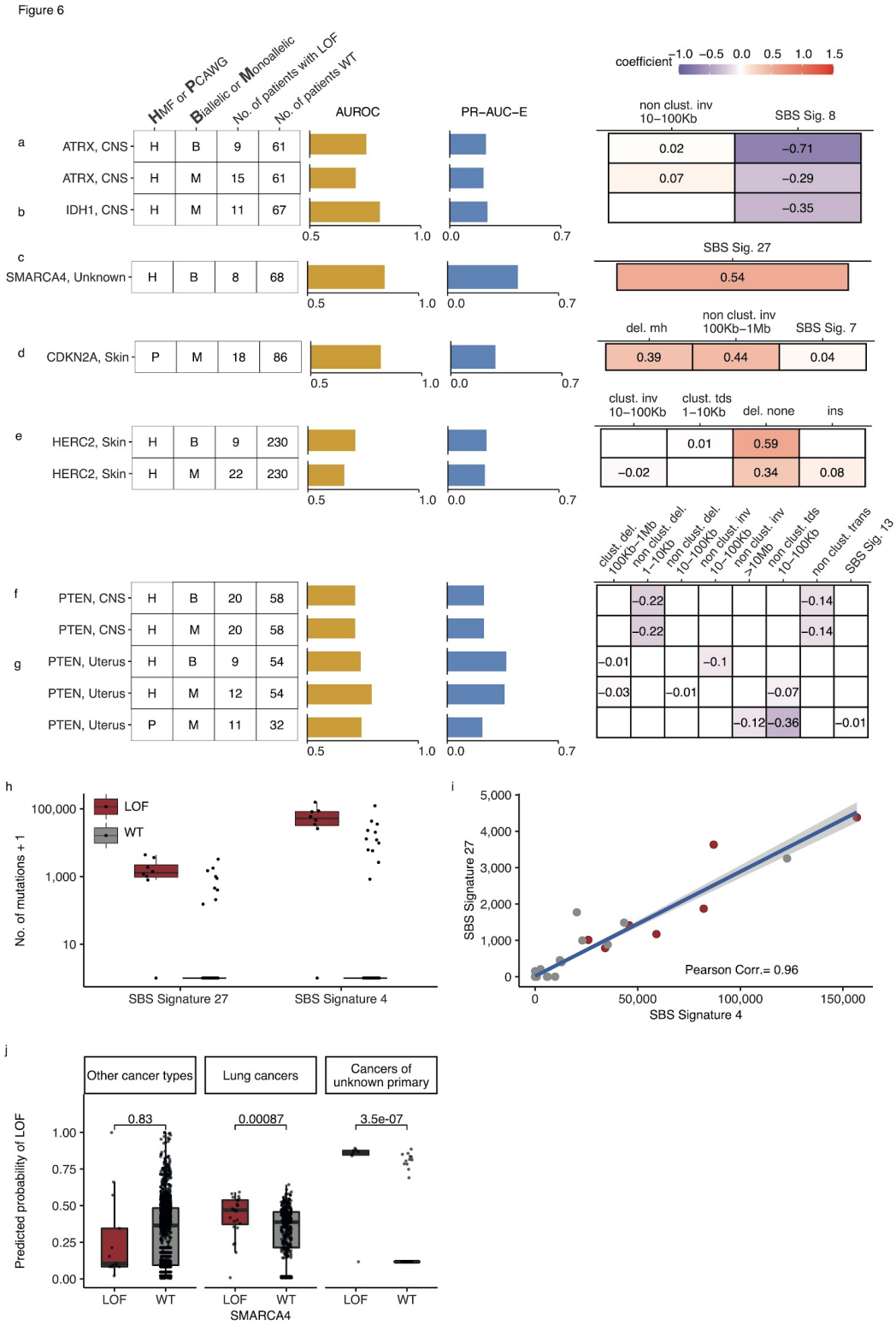

Figure 6: Novel predictive models of DDR gene deficiencies

a Predictive model of *ATRX*-d and its PR-AUC-E, AUROC, and selected features and their

975 coefficients. Same information for predictive models of (**b)** *IDH1*-d, (**c**) *SMARCA4*-d, (**d**)
976 *CDKN2A*-d, (**e**) *HERC2*-d, and (**f**) *PTEN*-d in CNS cancers and (**g**) uterine cancers.
977 **h** Number of SBS sig. 27 and SBS sig. 4 (y-axis; logarithmic) among tumours of unknown
978 primary with *SMARCA4* biallelic LOF (red) or wild-type (grey). **i** Pearson correlation between the
979 per-tumour number (tumours of unknown primary; HMF) of SBS signature 27 (y-axis) and SBS
980 signature 4 (x-axis; logarithmic) mutations, with an overlaid linear model (blue) and its 95%
981 confidence interval (grey). **j** Using a model trained to predict *SMARCA4* biallelic LOF in HMF
982 cancers of unknown primary, we evaluate the predictive power across cohorts (one-tailed
983 Wilcoxon rank-sum test) displaying significant cohorts separately (colours as in **a**).

984 Additional files

985 Additional file 1: Supplementary tables 1,2 and 4-9; Microsoft Excel (xlsx)

986 Additional file 1, Supplementary Table 1: All included tumours and their primary tumour
987 locations

988 Additional file 1, Supplementary Table 2: 736 DDR genes, hg19 coordinates and the number of
989 pathogenic events across 6,065 cancer genomes

990 Additional file 1, Supplementary Table 5: Proposed Etiologies of base substitution signatures

991 Additional file 1, Supplementary Table 6: All models (n=535)

992 Additional file 1, Supplementary Table 7: Shortlisted models (n=48)

993 Additional file 1, Supplementary Table 8: Pathogenic events in each of the 535 LOF-sets

994 Additional file 1, Supplementary Table 9: Correlation between features in shortlisted models

995

996 Additional file 2: Supplementary table 3-4; zip-compressed; tab-separated values (.tsv), may be
997 opened in Microsoft Excel

998 Additional file 1, Supplementary Table 3: All SBS signature contributions, indels counts, and SV
999 counts, per sample

1000 Additional file 1, Supplementary Table 4: All SBS signature contributions, indels counts, and SV
1001 counts, per sample, log-transformed and scaled to z-scores

1002

1003 Additional file 3: Supplementary text; pdf (.pdf)

1004 Supplementary Text: Significant models that are not described in the main text

1005

1006 Additional file 4: Supplementary figures; pdf (.pdf)

1007 Supplementary Fig. 1: Shortlisted predictive models of DDR gene deficiencies not included in
1008 the main manuscript

1009 Supplementary Fig. 2: *CDKN2A*-d in PCAWG and HMF skin cancers, *HERC2*-d in HMF skin

1010 cancers, and *ARID1A*-d in PCAWG prostate cancers